JOURNAL OF GEOPHYSICAL RESEARCH, VOL. 115, D14121, doi:10.1029/2009JD013181, 2010

Influence of the 2006 Indonesian biomass burning aerosols on tropical dynamics studied with the GEOS-5 AGCM

Lesley Ott,[1] Bryan Duncan,[2] Steven Pawson,[3] Peter Colarco,[2] Mian Chin,[2] Cynthia Randles,[1] Thomas Diehl,[1] and Eric Nielsen[4]

Received 10 September 2009; revised 5 February 2010; accepted 2 March 2010; published 30 July 2010.

[1] The direct and semidirect effects of aerosols produced by Indonesian biomass burning (BB) during August–November 2006 on tropical dynamics have been examined using NASA's Goddard Earth Observing System, version 5, (GEOS-5) atmospheric general circulation model (AGCM). Simulations were driven by two sets of aerosol forcing fields calculated offline by a separate aerosol transport model, one that included Indonesian BB aerosol emissions and one that did not. In order to separate the influence of the aerosols from internal model variability, the means of two ten-member ensembles were compared. Diabatic heating from BB aerosols increased temperatures over Indonesia between 150 and 400 hPa. The higher temperatures resulted in strong increases in upward grid-scale vertical motion, which increased water vapor and CO over Indonesia. In October, the largest increases in water vapor were found in the midtroposphere (~25%) while the largest increases in CO occurred just below the tropopause (80 ppbv or ~50%). Diabatic heating from the Indonesian BB aerosols caused CO to increase by 9% throughout the tropical tropopause layer in November and 5% in the lower stratosphere in December. The results demonstrate that aerosol heating plays an important role in the transport of BB pollution and troposphere-to-stratosphere transport. Changes in vertical motion and cloudiness induced by aerosol heating can also alter the transport and phase of water vapor in the upper troposphere/lower stratosphere.

Citation: Ott, L., B. Duncan, S. Pawson, P. Colarco, M. Chin, C. Randles, T. Diehl, and E. Nielsen (2010), Influence of the 2006 Indonesian biomass burning aerosols on tropical dynamics studied with the GEOS-5 AGCM, *J. Geophys. Res.*, *115*, D14121, doi:10.1029/2009JD013181.

1. Introduction

[2] The black and organic carbon aerosols from forest and agricultural fires can have significant impacts on radiative forcing, atmospheric composition, and atmospheric dynamics, especially for fires with high biomass loadings. Tropical peatlands in Indonesia store large amounts of carbon (55 ± 10 Gt of carbon [*Jaenicke et al.*, 2008]). Intact peatlands support swamp forests overlying peat deposits which extend up to 20 m in depth but conversion for agricultural land use has resulted in the burning of large areas of peatlands [*Page et al.*, 2002]. In drought conditions brought on by El Niño [e.g., *van der Werf et al.*, 2003; *Wang et al.*, 2004; *Logan et al.*, 2008] or the Indian Ocean Dipole [*Field et al.*, 2009], deliberately set fires can spread out of control, consuming underlying peat deposits in addition to above ground forest biomass and resulting in large fluxes of carbon to the atmosphere.

[3] During one of the largest burning events of the Twentieth Century, the Indonesian wildfires of 1997 (August–November), the aerosol radiative forcing at the surface was estimated to be −10 to −50 W/m^2 over the ocean near Indonesia, −5 to −50 W/m^2 over the central Indian Ocean, and as low as −150 W/m^2 over the land where burning occurred [*Duncan et al.*, 2003; *Podgorny et al.*, 2003]. *Duncan et al.* [2007a] used the Global Modeling Initiative (GMI) chemical transport model (CTM) to estimate that these fires increased CO in the tropical tropopause layer (TTL) by more than 40% and lower stratosphere (LS) by more than 10% for several months. Their results also demonstrated that the increased presence of CO resulting from the Indonesian wildfires could reduce OH mixing ratios, increasing atmospheric lifetimes and troposphere-to-stratosphere transport of trace gases.

[4] Another, smaller, wildfire outbreak occurred from August to November 2006 and is the focus of this study. *Logan et al.* [2008] used data from the Tropospheric Emissions Spectrometer (TES) to assess differences in O_3, CO, and water vapor between 2005 and 2006. Their results

[1]Goddard Earth Sciences and Technology Center, University of Maryland, Greenbelt, Maryland, USA.
[2]Atmospheric Chemistry and Dynamics Branch, NASA Goddard Space Flight Center, Greenbelt, Maryland, USA.
[3]Global Modeling and Assimilation Office, NASA Goddard Space Flight Center, Greenbelt, Maryland, USA.
[4]Science Systems and Applications, Inc., Lanham, Maryland, USA.

0148-0227/10/2009JD013181

indicated that CO mixing ratios at 511 hPa were more than 80 ppbv greater in October and November of 2006 relative to the same months in 2005 over the Indonesian region; ozone mixing ratios were 15–30 ppbv (30–75%) larger. *Ziemke et al.* [2009] used satellite observations and the GMI model to estimate that BB increased tropospheric ozone mixing ratios in the Indonesian region by 15–25% during the 2006 event. *Chandra et al.* [2009] used the GMI model to separate the dynamical impact of the 2006 El Niño from changes in BB emissions. They found that emissions and dynamical changes contributed almost equally to observed ozone increases over Indonesia in October and November, though changes because of emissions were focused in the Indonesian region while dynamical changes affected a larger area in the Indian and Pacific Oceans. The global burden of CO increased by 8–12% from October through December as a result of the 2006 fires [*Chandra et al.*, 2009].

[5] In addition to modifying atmospheric composition, BB aerosols alter the atmospheric circulation in several ways. Black carbon (BC) aerosol absorbs incoming solar radiation, while organic carbon (OC) and sulfate aerosol both scatter and absorb (direct effect). The aerosol indirect effect refers to the influence of aerosols on cloud formation and optical properties through microphysical processes. In addition to direct and indirect effects, aerosols that absorb incoming solar radiation can alter atmospheric heating rates, changing the properties and lifetimes of clouds as well as vertical distributions of temperature and moisture (semidirect effect). *Ming and Ramaswamy* [2009] used the AM2.1 atmospheric general circulation model (AGCM) which includes aerosol direct, semidirect and indirect effects and found that increasing aerosols from preindustrial to 1990 levels caused a decrease in the global annual mean surface temperature of 1.9 K. While cooling the troposphere, the increase in aerosols typically warmed the stratosphere. *Menon et al.* [2002] and *Randles and Ramaswamy* [2008] found that absorbing carbonaceous aerosol associated with the "Atmospheric Brown Cloud" [*Ramanathan and Crutzen*, 2003] over Asia increases diabatic heating and contributes to enhanced upward motion, a strengthening of the monsoon circulation, and increased precipitation in parts of Asia during the premonsoon period, a mechanism referred to as the "Elevated Heat Pump" [*Lau et al.*, 2006; *Lau and Kim*, 2006]. Increased diabatic heating associated with aerosols may also induce convection and lead to cloud formation, which contributes to the surface solar flux reduction [*Rudich et al.*, 2003; *Randles and Ramaswamy*, 2008]. Reduction in solar flux to the surface because of aerosols and clouds weakens the north-south temperature gradient, which ultimately leads to a weakening of the monsoon [*Chung and Ramanathan*, 2006]. *Rajeev et al.* [2008] studied the impact of the 1997 Indonesia wildfires on sea surface temperature (SST) using satellite observations of aerosol optical depth, SST, and a radiative transfer model. They found that aerosol cooling resulted in a 1 to 2°C negative SST anomaly in the eastern equatorial Indian Ocean though the impact likely would have been larger had decreased cloud cover during this period not resulted in a positive anomaly in net cloud radiative forcing. The decrease in SSTs resulting from BB aerosols may have contributed to a strengthening of the Indian Ocean Dipole.

[6] In this study, we examine the impact of the direct and semidirect effects of sulfate and carbonaceous aerosols from the 2006 Indonesian fires on tropical dynamics using the Goddard Earth Observing Systsem, Version 5 (GEOS-5) AGCM. Though the chemical effects of these fires have been studied extensively, the influence of changes in radiative heating on atmospheric circulation has not been examined. Simulations that do and do not include the radiative effects of these aerosols are compared in order to estimate changes to horizontal and vertical transport, temperature, water vapor, and CO mixing ratios in the Indonesian region. An ensemble methodology is used to separate the role of aerosol forcing from the potentially chaotic response of the model to perturbations. Ten-member ensembles with and without Indonesian aerosols were produced by initializing simulations with meteorological fields taken from different days in April 2006. Section 2 includes details on the GEOS-5 AGCM while section 3 describes the methodology used in this study. Section 4 presents results from the ensemble simulations and section 5 includes a summary and conclusions. Section 6 contains concluding remarks.

2. GEOS-5 AGCM Description

[7] The GEOS-5 AGCM is a central component of the GEOS-5 atmospheric data assimilation system [*Reinecker et al.*, 2008], where it is used for meteorological analysis and forecasting [*Zhu and Gelaro*, 2008]. By adding trace gases and aerosol modules, GEOS-5 has also been developed as a tool for studying atmospheric composition and climate. L. E. Ott et al. (An analysis of the impact of convective parameter sensitivity on simulated global atmospheric CO distributions, in preparation for *Atmospheric Chemistry and Physics*, 2009) used ensemble simulations of GEOS-5 to quantify the impact of changes in the model's moist physics code on global CO distributions.

[8] The AGCM combines a finite volume dynamical core [*Lin*, 2004] with a column physics package and the land-surface model of *Koster et al.* [2000]. The model domain extends from the surface to 0.01 hPa and uses 72 hybrid sigma-P layers that transition from terrain-following near the surface to pure pressure levels above 180 hPa. In this study, the AGCM was used with a horizontal resolution of 1° by 1.25° (latitude by longitude). Physics computations are performed every 30 min.

[9] The column physics model contains several components. Boundary layer turbulence is represented using the *Lock et al.* [2000] scheme. Moist processes in GEOS-5 are represented by a convective parameterization and a prognostic cloud scheme. Convection is parameterized using the relaxed Arakawa-Schubert (RAS) scheme of *Moorthi and Suarez* [1992], a modified version of the Arakawa-Schubert scheme [*Arakawa and Schubert*, 1974], in which the atmosphere is relaxed toward equilibrium. The prognostic cloud scheme contained in GEOS-5 calculates large-scale ice and liquid condensate by assuming a probability distribution function (pdf) of total water. Condensate is removed from the domain by evaporation, autoconversion of liquid condensate, sedimentation of frozen condensate, and accretion of condensate by falling precipitation. Radiation transfer is computed using the parameterization of *Chou and*

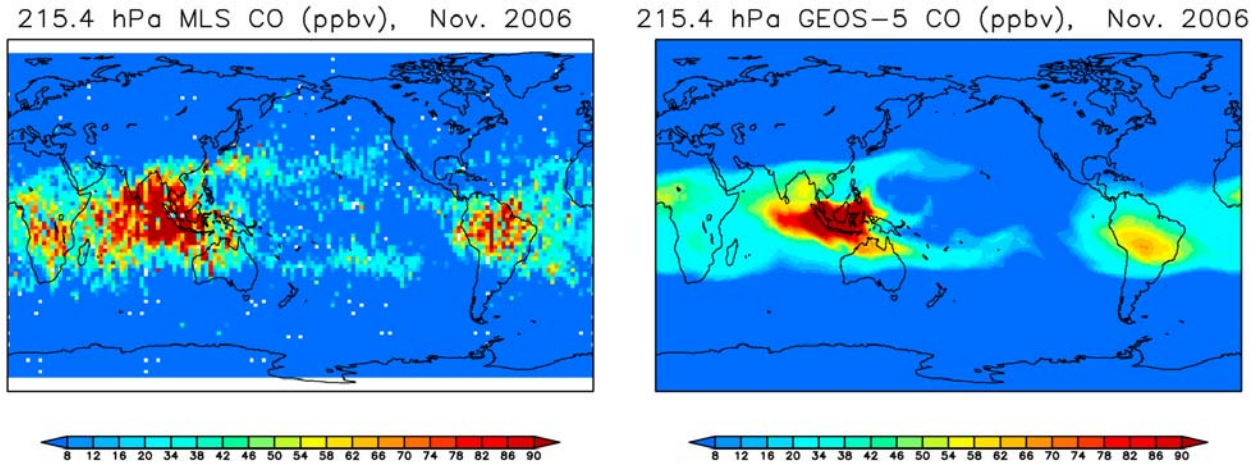

Figure 1. November 2006 (left) Microwave Limb Sounder (MLS) CO perturbation mixing ratios at 215.4 hPa and (right) Goddard Earth Observing System, version 5, (GEOS-5) simulated CO mixing ratios in ppbv (calculated by subtracting the MLS global mean from observed MLS CO mixing ratios and subtracting the GEOS-5 global mean from simulated GEOS-5 CO mixing ratios). GEOS-5 CO at 215.4 hPa is calculated by averaging CO over 5 model layers (~4 km) in order to approximate the vertical resolution of MLS.

Suarez [1994, 2002] and *Chou et al.* [2003]. The model accounts for the radiative effects of sulfate, dust, sea salt, organic carbon and black carbon aerosol. For this study, two different three-dimensional aerosol distributions were specified in the AGCM.

[10] The GEOS-5 AGCM has been adapted to include several atmospheric chemistry modules: this study uses a version with a simple representation of CO. Emissions of CO follow *Duncan et al.* [2007a] and *Duncan and Logan* [2008]. Relevant to this study, CO emissions from biofuels follow the *Yevich and Logan* [2003] inventory while BB emissions follow the Global Fire Emissions Database, version 2 (GFEDv2) inventory [*van der Werf et al.*, 2006]. All simulations include BB emissions of CO from Indonesia to isolate the effects of aerosol heating on trace gas distributions. In this study, we use a CO-only simulation similar to the one described in *Duncan et al.* [2007b], which we briefly describe here. CO emissions from fossil fuels, biofuels, and BB are increased by 20%, 19%, and 11%, respectively, in order to account for CO production from nonmethane hydrocarbons emitted from these sources. Isoprene and monoterpene emissions were calculated by the GMI combined troposphere-stratosphere CTM using the method of *Guenther et al.* [1995] and are released directly as CO after applying an estimated yield during the oxidation of these species. Monthly mean methane fields are used to calculate CO produced by methane oxidation as described in *Bian et al.* [2007]. In order to calculate CO loss through reaction with OH, monthly mean OH fields produced by the GMI CTM for the year 2006 are used along with a prescribed loss frequency for CO.

[11] Figure 1 shows a comparison of CO, a tracer of transport and fire pollution, in the upper troposphere (UT) as observed by the Microwave Limb Sounder (MLS, version 2/level 2 [*Livesey et al.*, 2008]) instrument onboard the NASA Aura satellite and modeled by GEOS-5. Though this MLS data product is known to be biased high at 215.4 hPa [*Livesey et al.*, 2008], it has been used previously to qualitatively validate simulated CO distributions [e.g., *Duncan et al.*, 2007a]. The model captures the main features of transport to and within the UT that are evident in the observations. The long-range transport pathways of the pollution from the 1997 Indonesian fires are detailed in *Duncan et al.* [2003] and *Duncan et al.* [2007a]; these pathways are similar to those of the 2006 event. Areas of monsoonal convection near the main burning regions in Africa, South America and Indonesia loft fire pollutants to the UT where they are transported by the prevailing tropical easterlies. Some of the pollution is peeled away by the subtropical jets, moving rapidly eastward and circling the globe. This feature is best seen over the Pacific Ocean in Figure 1. To our knowledge, these MLS CO measurements are the first satellite observations to show this long-range transport of fire pollution within the subtropical jets.

[12] *Jiang et al.* [2010] compared five years (2004–2009) of upper tropospheric MLS water vapor and cloud ice observations with meteorological analyses from the GEOS-5 data assimilation system. At 215 and 147 hPa, GEOS-5 was able to reproduce the observed morphology of moisture, thought the model overestimated water vapor by 50% at 215 hPa and 30% at 147 hPa. Simulated and observed IWC generally agreed within 15% at these levels. At 100 hPa, water vapor was underestimated in the tropics and overestimated in the extratropics while IWC was less than observed, globally. *Jiang et al.* [2010] also compared MLS observed temperatures with temperatures from the GEOS-5 analysis. Their results indicated that GEOS-5 tropical temperatures tended to be warmer by ~3 K compared to MLS observations at 215 hPa and by ~1.5 K at 147 hPa. However, because MLS is known to have a low bias in tem-

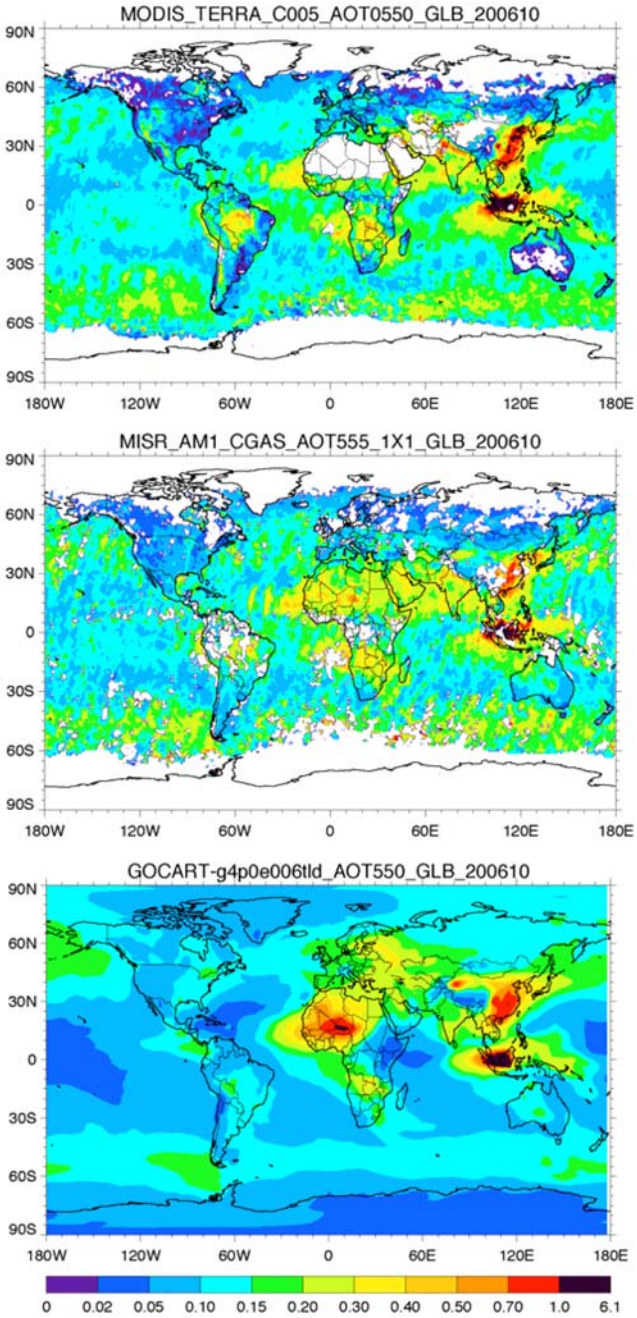

Figure 2. Distributions of monthly mean aerosol optical depth observed by (top) Moderate Imaging Spectroradiometer (MODIS) and (middle) Multiangle Imaging Spectroradiometer (MISR) aboard the Aqua satellite and (bottom) simulated by the Goddard Chemistry Aerosol Radiation and Transport (GOCART) model during October 2006. MODIS and MISR data are cloud-free and collected with a 1030 local overpass time. The GOCART monthly mean is calculated using all times during October 2006.

perature in cloudy regions [*Schwartz et al.*, 2008] the overestimation of tropical temperatures in GEOS-5 is likely to be smaller (~1 K) at 215 and 147 hPa. At 100 hPa, GEOS-5 temperatures agreed well with observations. The *Jiang et al.* [2010] study demonstrates that GEOS-5 is able to reasonably reproduce observed patterns of upper tropospheric temperature and moisture.

3. Methodology

[13] This section describes two important aspects of the experimental design: the construction of the aerosol distributions specified in GEOS-5 and the use of ensembles of GEOS-5 simulations to separate physical signals from statistical variations.

3.1. Aerosol Distributions

[14] By using specified aerosol fields to force GEOS-5, we are able to isolate the radiative impacts of aerosols on dynamics without considering the complex feedbacks of dynamics on aerosol distributions. This could include alteration of horizontal and vertical advection, removal by precipitation, and transport in convective updrafts. Aerosol indirect effects are also neglected in this study.

[15] Two aerosol distributions, including and excluding the impacts of the Indonesian BB emissions, were constructed for the GEOS-5 AGCM experiments. They were computed from runs made with the Goddard Chemistry Aerosol Radiation and Transport (GOCART) model [*Chin et al.*, 2002] driven by meteorological analyses from the GEOS-4 data assimilation system for 2006. Details on the aerosol optical properties used in the GOCART calculations are provided in *Chin et al.* [2009]. BC, OC, and SO_2 emissions from fires were specified according to the GFEDv2 inventory [*van der Werf et al.*, 2006]. Figure 2 shows a comparison between October 2006 GOCART simulated aerosol optical depth (AOD) and AOD observed by Moderate Imaging Spectroradiometer (MODIS) and Multiangle Imaging Spectroradiometer (MISR). In the Indonesian region, the distribution of simulated AOD compares well with observations from both MODIS and MISR. The model is also able to capture the spatial pattern of transport of biomass burning aerosol over the Pacific and Indian Oceans.

[16] *Yu et al.* [2010] compared the vertical distribution of GOCART calculated aerosols during this period with observations obtained by Cloud-Aerosol Lidar and Infrared Pathfinder Satellite Observations (CALIPSO). Seasonal mean AOD from GOCART for September–November (SON) of 2006 compared well with CALIPSO observations with a mean AOD of 0.16 calculated from both products over a region including Indonesia, parts of northern Australia, and southeast Asia. Both CALIPSO and GOCART AOD were lower than AOD from the MODIS over the same region (0.22). The vertical distributions of simulated and observed aerosols were also examined by *Yu et al.* [2010] by calculating the aerosol-scale height, defined as the altitude above ground level below which 63% of the total AOD is present. A comparison of seasonal mean aerosol-scale heights calculated from CALIPSO and GOCART suggests that GOCART consistently overestimates the aerosol-scale height relative to CALIPSO although in the Indonesian region, these differences are less than 0.5 km.

[17] In addition, *Chin et al.* [2009] studied light absorption by pollution, dust, and biomass burning aerosols using an 8 year (2000–2007) GOCART simulation and compared the model results with observations from the AERONET surface Sun photometer network. The results indicated that

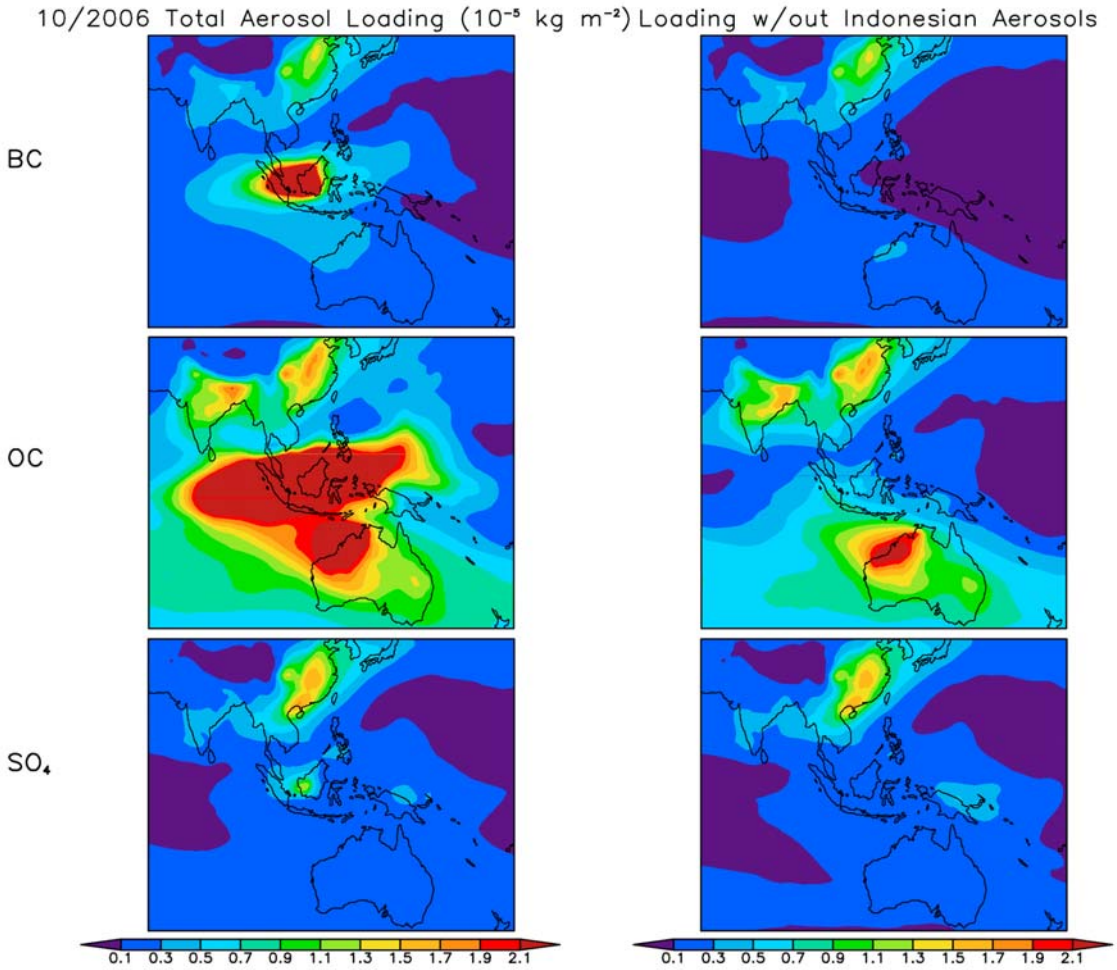

Figure 3. Column loading (10^{-5} kg m^{-2}) of (top) black carbon (BC), (middle) organic carbon (OC), and (bottom) sulfate aerosol produced by GOCART chemical transport model simulations and used to force the (left) AERO and (right) NAERO GEOS-5 ensembles. The fields shown are for October 2006.

simulated AOD compared well with observations, both globally and regionally, though AOD from biomass burning aerosols was often underestimated by 30–40%. The model showed less skill in predicting absorption optical depth and single scattering albedo (SSA). At Lake Argyle in northern Australia, the average GOCART calculated SSA at 550 nm was 0.87 while the SSA calculated from AERONET data was only 0.83. The results are likely representative for 2006, though calculated over the 8 year period from 2000 to 2007, because the composition of the biomass burning aerosol shows little variability despite large interannual variations in AOD. The disparity in simulated and observed SSA indicates that GOCART simulated aerosols are less absorbing than aerosols observed by AERONET over Australia. If this conclusion is also true in the Indonesian region, it may cause the GCM simulations to underestimate aerosol-induced changes in atmospheric heating rates and the dynamical response to aerosol heating.

[18] Two GOCART model integrations were performed to produce the aerosol forcing fields used by GEOS-5. One simulation (AERO) included all BB emissions specified by the GFEDv2 inventory for BC, OC, and SO_2 while the second simulation (NAERO) was identical, expect that it omitted those sources contained in Indonesian land grid boxes. Both simulations were driven with identical GEOS-4 DAS meteorological fields for 2006. Figure 3 shows the difference in column aerosol loading between the two sets of aerosol fields for BC, OC, and sulfate during October. For sulfate aerosol, the absence of Indonesian emissions is noticeable primarily over Indonesia. BC and OC aerosols from Indonesia affect a larger region with high aerosol loadings extending thousands of kilometers into the Pacific and Indian Oceans.

[19] Figure 4 shows the mean vertical distribution during SON 2006 and annual cycle of total aerosol mass in the Indonesian region (100° to120°E and 10°S to 10°N). OC dominates the aerosols emitted from the fires with the greatest concentrations found near the surface. *Thampi et al.* [2009] analyzed CALIPSO observations of the 2006 Indonesian smoke plume and found that the majority of aerosols remained below 3 km which is consistent with the vertical distribution calculated by GOCART. Though mixing ratios are much smaller than at low levels, significant amounts of aerosol are present in the midtroposphere and upper tropo-

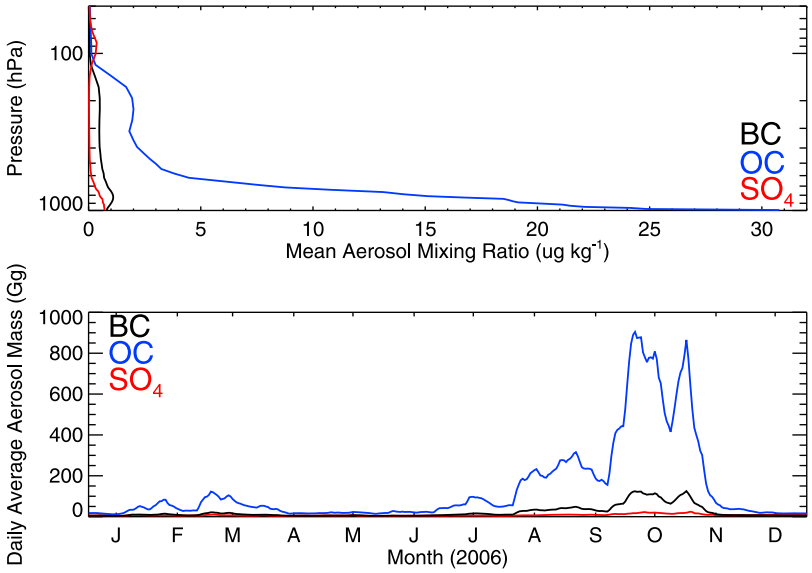

Figure 4. Aerosol distributions over Indonesia used in the AERO simulations. (top) Vertical distributions of BC (black line), OC (blue line), and sulfate (red line) aerosol mass mixing ratios calculated during SON 2006 over the Indonesian region (100° to 120°E and 10°S to 10°N). (bottom) Annual cycle of total aerosol mass for each of the three aerosol types over the Indonesian region.

sphere. Total aerosol mass in the region begins to increase in August with peaks in October and early November.

3.2. GEOS-5 Ensembles

[20] It is necessary to use an experimental strategy that can isolate significant impacts of BB aerosols on the circulation, in the sense that the impact of the aerosol forcing is larger than the "natural variability" of the atmosphere. For this study, this has been achieved using ensembles of simulations.

[21] The AERO and NAERO aerosol fields produced by GOCART were used to force two ten-member ensembles of GEOS-5 AGCM simulations. Aerosol distributions were read in daily and interpolated to the 30 min model time step. Simulations in each ensemble were initialized using meteorological fields from 1, 3, 5, 7, 9, 11, 13, 15, 17, and 19 April in order to introduce variability. Nine-month model integrations began in April 2006 to allow the impact of the difference in initial condition to develop prior to the period of burning (August through November) and ended in December 2006. The AGCM was run in climate mode in which Reynolds analyzed SSTs [*Reynolds et al.*, 2007] are prescribed but no atmospheric data are assimilated. Even without data assimilation, the strong control exerted by the SST anomalies on the atmosphere means that simulations are able to capture the major transport features of the 2006 El Niño in the tropical atmosphere.

[22] It is important to note that because observed SSTs were used as input to the model, the ensemble of simulations in which the Indonesian aerosol source was removed cannot be considered to be without the influence of these aerosols. *Rajeev et al.* [2008] analyzed observed SSTs to estimate that aerosol cooling associated with the 1997 Indonesian wildfires decreased SSTs in parts of the Indian Ocean 1–2°C though the impact would likely have been greater if changes in cloud cover had not also occurred.

[23] A number of studies have demonstrated the importance of ensemble size in separating responses of the climate system to perturbations from internal model variability or "noise" [e.g., *Taschetto and England*, 2008; *Wehner*, 2000]. In order to separate differences between the AERO and NAERO ensembles caused by Indonesian aerosols from noise, we use the Student's t test statistic which takes into account the means and standard deviations of both ensembles. The Student's t test has frequently been used to determine the significance of differences between ensembles of GCM simulations [e.g., *Vitart et al.*, 1997; *Li*, 1999; *Huebener et al.*, 2007; *Hargreaves et al.*, 2007]. In this study, differences are considered significant if they meet or exceed the 95% confidence level. To calculate profiles of changes induced by aerosols, we calculate the area mean change in a variable including all grid cells from 100° to 120°E and from 10°S to 10°N. We also calculate this quantity including only those grid cells in which differences are considered statistically significant in the sum but dividing over the same area. This quantity gives an indication of how much of the profile of differences between the AERO and NAERO ensembles can be considered statistically significant; the similarity of the two profiles indicates the relative significance of the changes in the Indonesian region.

4. Results

4.1. Radiative forcing

[24] Figure 5 shows the radiative forcing (change in net irradiance [*Ramaswamy et al.*, 2001]) resulting from Indonesian fire aerosols at the surface and top of the atmosphere (TOA). Aerosol radiative forcing is calculated for both the AERO and NAERO simulations assuming clear sky conditions meaning that the effects of clouds which may be present in the model are not included in the radiative forcing

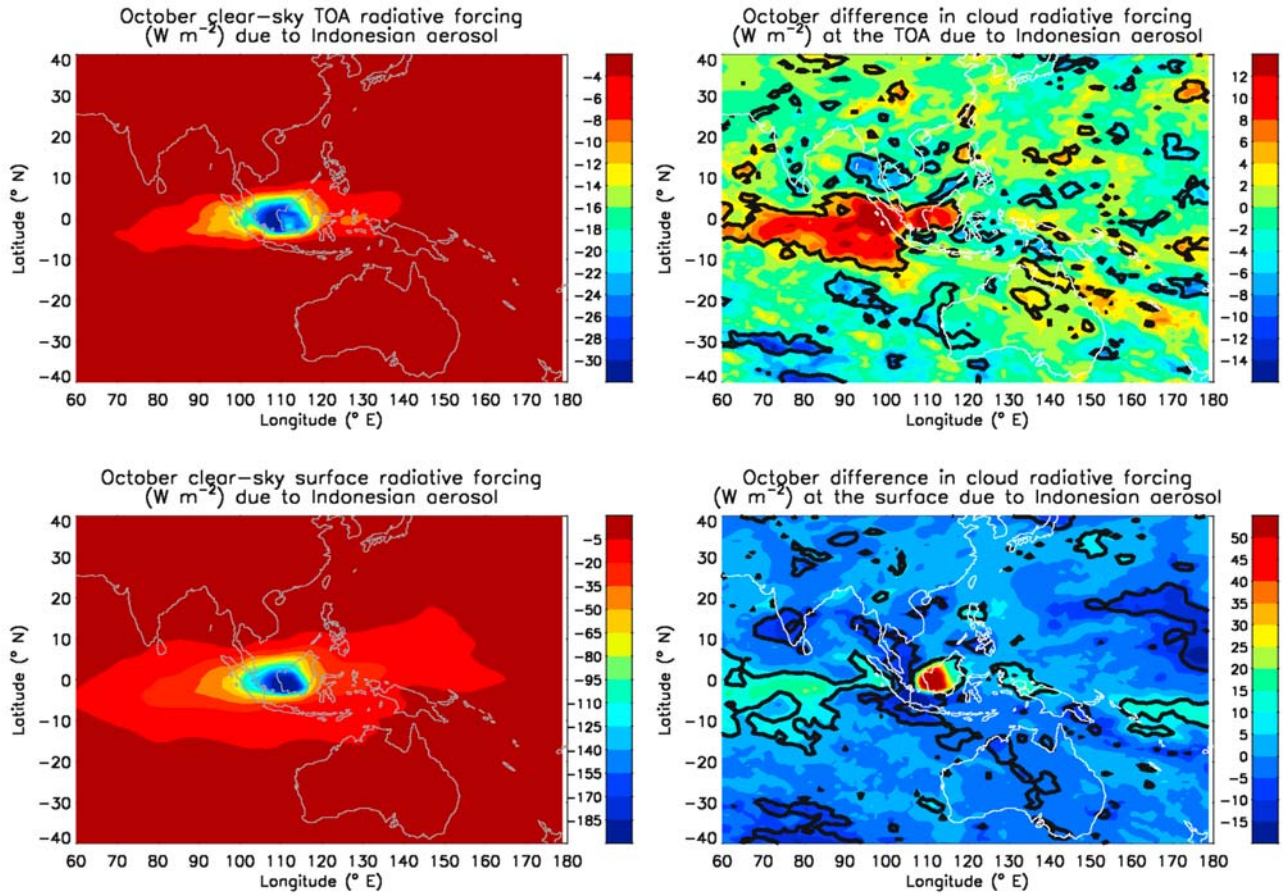

Figure 5. (top left) Clear-sky radiative forcing at the top of the atmosphere (TOA) and (bottom left) surface resulting from Indonesian aerosols calculated using GOCART AERO and NAERO aerosol distributions. Radiative forcing because of changes in cloudiness associated with Indonesian aerosols at the (top right) TOA and (bottom right) surface calculated by subtracting the NAERO ensemble mean from the AERO ensemble mean. Black contours indicate regions where the Student's t test indicates differences between ensembles are statistically significant at the 95% confidence level.

calculations. Cloud radiative forcing is calculated using the difference between radiative forcing with and without the influence of clouds. The influence of Indonesian fire aerosols on both cloud and aerosol radiative forcing is identified by subtracting the NAERO radiative forcing from the AERO forcing. The inclusion of aerosols emitted from Indonesia results in direct radiative forcings at the TOA as low as −30 W m^{-2} over areas of Kalimantan and the Karimata Strait. Areas of direct radiative forcing at the TOA as low as −6 W m^{-2} extend several thousand kilometers into the Indian Ocean. The change in ensemble mean cloud radiative forcing which results from including the aerosols was also calculated. The presence of Indonesian aerosols tends to increase cloud radiative forcing at the TOA with the largest increases (greater than 10 W m^{-2}) found in the Indian Ocean to the west of Indonesia. When the cloud and direct aerosol impacts are considered together, the magnitude is typically between 0 and −10 W m^{-2} over Kalimantan and the Karimata Strait and between 0 and 10 W m^{-2} over the Indian Ocean.

[25] Stronger impacts are seen in the surface energy balance. Direct radiative forcings as low as −220 W m^{-2} are found over Kalimantan. Over Kalimantan and Sumatra, direct radiative forcings are typically less than −50 W m^{-2} while large areas of the equatorial Indian and Pacific Oceans are subject to radiative forcings between −5 and −50 W m^{-2}. At the surface, positive cloud radiative forcings exceed 50 W m^{-2} over a small area on Kalimantan. Changes in cloudiness have a smaller but statistically significant impact over parts of the Indian Ocean. When cloud and clear-sky radiative forcings are considered together, peak radiative forcing at the surface is −160 W m^{-2}.

[26] The impact of clouds on radiative forcing differs at the TOA and surface in both magnitude and geographical extent. Indonesian aerosols cause strong increases in low-level cloud cover (greater than 40%), though these changes are strongly localized. Peak increases in cloudiness are smaller at mid and high levels (~25 and 20%, respectively), but extend over larger areas to the south and west of the burning region. Cloud radiative forcings reflect the changes in cloud fraction caused by Indonesian aerosols. At the surface, increases in radiative forcing most strongly reflect changes in low-level cloudiness with large changes concentrated in the burning area; at the TOA, weaker but more expansive changes in cloud cover at mid and high levels

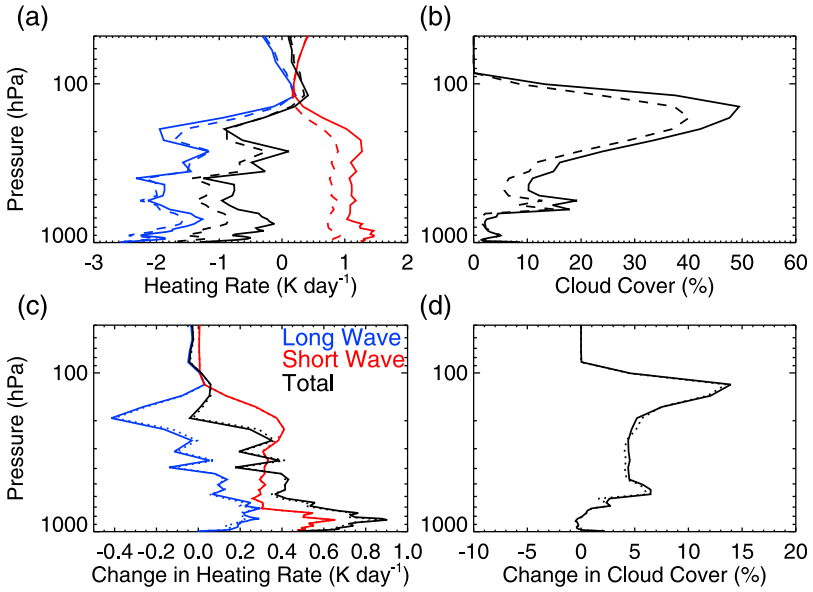

Figure 6. (a) Long-wave (blue line), short-wave (red line), and total (black line) radiative heating rates and (b) percentage cloud cover in the AERO (solid line) and NAERO (dashed line) ensembles during October 2006. All quantities are averaged over grid cells between 100° to 120°E and 10°S to 10°N. (c) Changes in radiative heating rates and (d) cloud cover due to Indonesian aerosols (AERO ensemble mean minus NAERO ensemble mean). Solid lines in Figures 6c and 6d indicate profiles calculated over all grid cells in the region described above while dotted lines indicate profiles including only grid cells in which the Student's t test indicated statistically significant differences.

result in statistically significant cloud radiative forcings extending over a larger area. It should be noted that cloud radiative forcings reflect only the direct and semidirect aerosol effects; if aerosol indirect effects were simulated, cloud radiative forcings caused by Indonesian aerosol would likely be considerably different.

4.2. Temperature

[27] Figure 6 shows profiles of the changes in short- and long-wave heating rates and cloudiness in October caused by the simulation of aerosol direct and semidirect effects. Heating rate profiles, calculated from 100° to 120°E and 10°S to 10°N, include both cloud and aerosol heating effects. Indonesian BB aerosols result in short-wave heating throughout the atmosphere with the largest impact (greater than 0.4 K day^{-1}) found at low levels. A secondary peak is found in the UT. The profile of change in long-wave radiative heating largely reflects changes in cloudiness. The largest change in cloud cover occurs between 100 and 200 hPa. A small but statistically significant increase in cloudiness of 4–5% is found from 200 to 450 hPa while a slightly larger increase occurs in the layers between 450 and 600 hPa. The largest increases in long-wave radiative heating are found in the low-troposphere to midtroposphere, below the levels (~650–85 hPa) where cloud cover is most enhanced. Between 150 and 500 hPa, changes in cloud cover result in long-wave cooling with the greatest cooling of −0.45 K day^{-1} occurring at approximately 200 hPa.

[28] Strong increases in temperature occur in the mid-troposphere to upper troposphere between 150 and 400 hPa because of increased diabatic heating caused by Indonesian BB aerosols (Figure 7). In October, the difference in monthly mean temperature at these levels is greater than 0.5 K and only slightly smaller during November. Changes in temperature in September and December are smaller and less statistically significant. At the tropopause (118 hPa), strong cooling of 0.8 K is seen in October because of the presence of Indonesian aerosols along with a slight warming

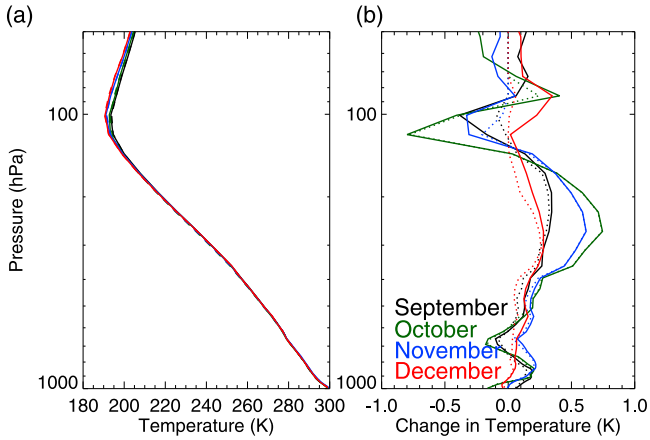

Figure 7. (a) Profiles of temperature in the AERO (solid line) and NAERO (dashed line) ensembles averaged over grid cells between 100° to 120°E and 10°S to 10°N during September (black), October (green line), November (blue line), and December (red line). (b) Changes in temperature because of Indonesian aerosols (AERO ensemble mean minus NAERO ensemble mean). Solid lines in Figure 7b indicate profiles calculated over all grid cells in the region described above while dotted lines indicate profiles including only grid cells in which the Student's t test indicated statistically significant differences.

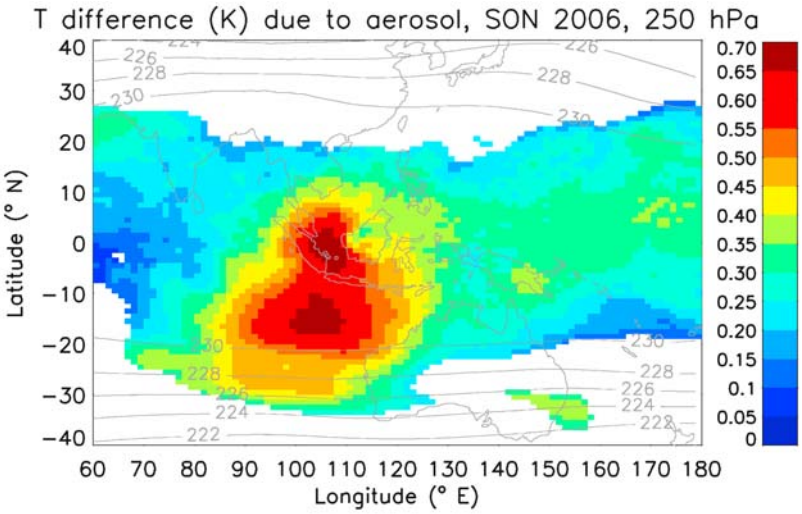

Figure 8. Average temperature difference during SON 2006 at 250 hPa resulting from simulating the effects of Indonesian BB aerosols (AERO ensemble mean minus NAERO ensemble mean). Only statistically significant (as indicated by the Student's t-test) grid column differences are shown. Grey contours show AERO ensemble-mean temperatures.

in the LS at 85 hPa. These effects will be discussed in more detail in section 4.6.

[29] Figure 8 shows the horizontal distribution of temperature change associated with the Indonesian BB aerosols during SON. The largest increases in temperature occur in the Indonesian region, over Sumatra and the Karimata Strait, and in an area to the south over the Indian Ocean. A similar pattern of temperature increase is found at 200 and 300 hPa. Warming over Indonesia is primarily driven by short-wave aerosol heating while warming to the south is associated with increased high-level cloudiness and latent heat release in addition to weaker aerosol heating effects. Though the largest impact on temperature is confined to Indonesia and the region directly to the south, warming averaging between 0.2 and 0.3 K is found over large areas of the Pacific Ocean.

4.3. Circulation

[30] Heating caused by Indonesian aerosols also alters atmospheric circulation. Figure 9 shows profiles of the changes in grid-scale vertical mass flux, convective mass flux, and divergence in the Indonesian region. Diabatic heating by aerosols causes large increases in buoyancy with air rising throughout the troposphere. The impact is strongest in October with the largest increase in vertical mass flux at 400 hPa. Changes in convective mass flux are considerably smaller and demonstrate less statistical significance. The largest increases in convective mass flux occur between 600 and 700 hPa. Small decreases in convective mass flux in October above 500 hPa suggest that the increase in shallow convection may come at the expense of deeper convection capable of reaching the midtroposphere to upper troposphere. *Dickerson et al.* [1997] noted that scattering aerosols tend to cool the boundary layer and stabilize the atmosphere with respect to convection. While absorbing aerosols in the boundary layer tend to destabilize the atmosphere, absorbing aerosols in the free troposphere increase stability [*Dickerson et al.*, 1997]. In the simulations presented here, convective available potential energy (CAPE) tends to decrease over Sumatra and Kalimantan when BB aerosols are simulated. Figure 7 shows that the greatest increases in temperature over Indonesia occur at ~250 hPa though the change in vertical mass flux is weaker at this level than at 400 hPa. This may be in part because warming of environmental air in the UT results in decreased buoyancy of air parcels lifted from below.

[31] Changes in grid-scale vertical motion are balanced by changes in the horizontal flow. In October, increased convergence occurs over Indonesia below 400 hPa. From 100 to 400 hPa, divergence increases with peak values found near 200 hPa. Increased divergence persists above the tropopause (118 hPa) while at 85 hPa, a small increase in convergence occurs. Changes in circulation tend to be strongly localized and coincide with the areas of peak radiative forcing indicated in Figure 5. Enhancements in vertical advective mass flux are focused over the Karimata strait at all levels. Above 500 hPa, small decreases in upward transport are found over Kalimantan which suggests that increased aerosol forcing shifts the area of ascending air slightly to the west. The largest increase in midlevel and low-level convergence and upper level divergence also tend to occur over the Karimata Strait.

4.4. Water Vapor

[32] The presence of Indonesian BB aerosols also alters the distribution of water vapor. Figure 10 shows the percentage change in specific humidity caused by changes in aerosol heating. Throughout the troposphere over Indonesia, aerosols increase the concentration of water vapor. Increases in buoyancy cause air to rise over Indonesia, bringing air with higher moisture content from lower altitudes. At low levels, this is balanced by increased convergence which replenishes the supply of moisture. In October, peak chan-

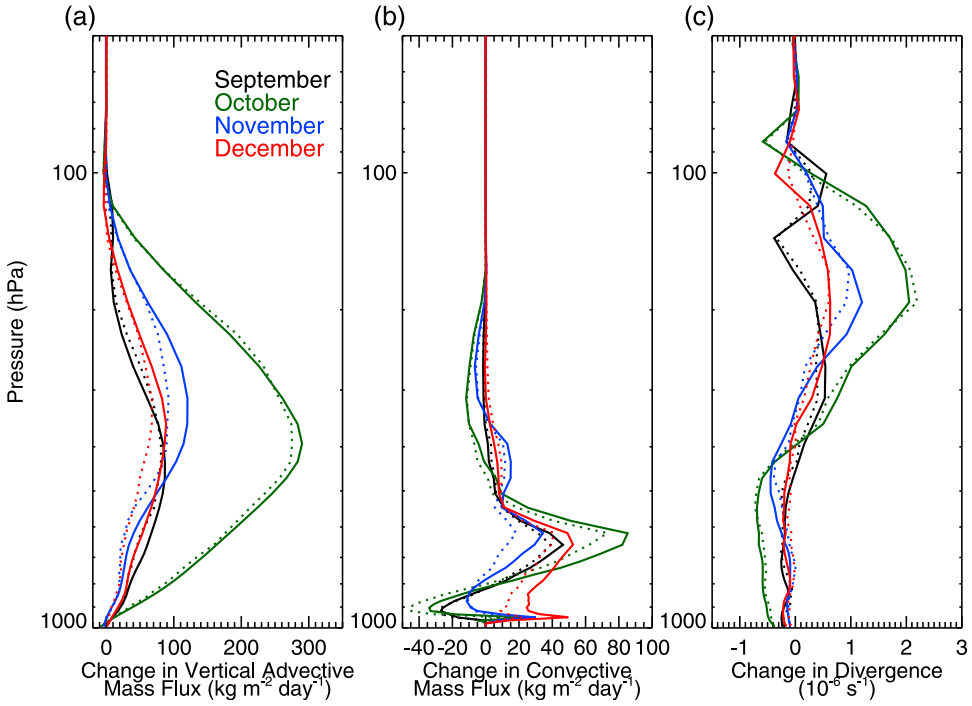

Figure 9. Changes in (a) vertical grid-scale mass flux, (b) convective mass flux, and (c) horizontal divergence because of Indonesian aerosols (AERO ensemble mean minus NAERO ensemble mean) in September (black line), October (green line), November (blue line), and December (red line). Solid lines indicate profiles calculated over all grid cells between 100° to 120°E and 10°S to 10°N while dotted lines indicate profiles including only grid cells in which the Student's t test indicated statistically significant differences.

ges occur in the midtroposphere to upper troposphere and can exceed 25% with a high degree of statistical significance. Specific humidity sharply decreases at the tropopause and in the layer above when Indonesian aerosol radiative effects are simulated. The evolution of these changes will be discussed in more detail in section 4.6. Figure 11 shows the horizontal distribution of water vapor changes induced by aerosols at 250 hPa for SON 2006. The largest impact is found over the Karimata Strait. Water vapor changes are more localized than temperature changes at this level and show little statistical significance outside of Indonesia.

[33] Changes in precipitation patterns also occur when the direct and semidirect effects of Indonesian aerosols are simulated, though these effects occur over a small region. Specifically, there is a decrease in precipitation over Kalimantan and an increase over the Karimata Strait. The difference in precipitation over the region (between 100°–120°E and 10°S–10°N) is approximately 19% during SON. However, because aerosol indirect effects were not simulated, it is not possible to estimate the total change in precipitation resulting from the Indonesian fires.

4.5. CO

[34] CO, in addition to water vapor, is strongly affected by changes in vertical and horizontal advection associated with Indonesian fire aerosols. Figure 12 shows monthly profiles of CO for the AERO and NAERO ensembles as well as profiles of the change in CO mixing ratios over the Indonesian region. Large increases in CO mixing ratio occur in

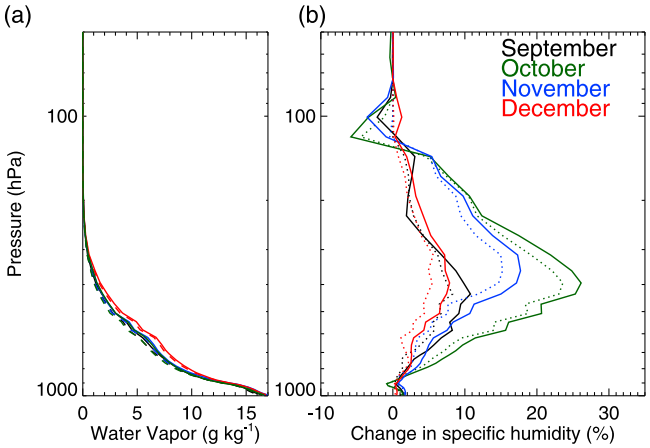

Figure 10. (a) Profiles of specific humidity in the AERO (solid lines) and NAERO (dashed lines) ensembles averaged over grid cells between 100° to 120°E and 10°S to 10°N during September (black line), October (green line), November (blue line), and December (red). (b) Changes in specific humidity because of Indonesian aerosols (AERO ensemble mean minus NAERO ensemble mean). Solid lines in Figure 10b indicate profiles calculated over all grid cells in the region described above while dotted lines indicate profiles including only grid cells in which the Student's t test indicated statistically significant differences.

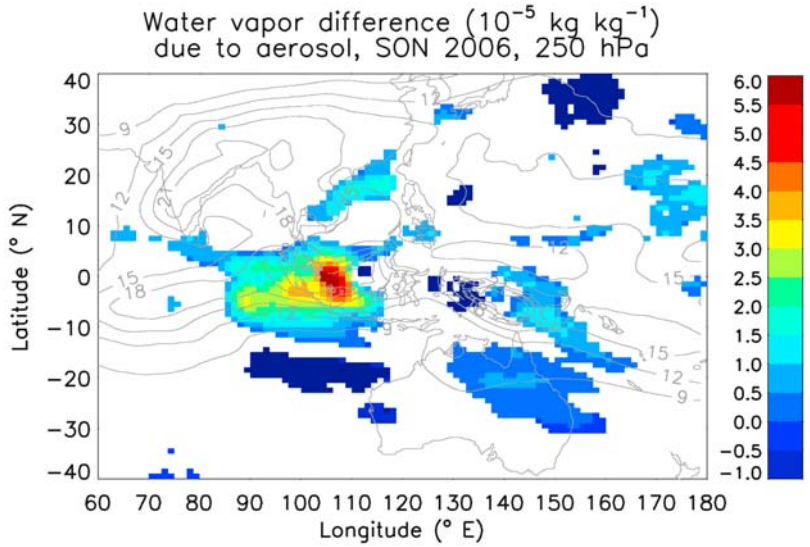

Figure 11. Average specific humidity difference during SON 2006 at 250 hPa resulting from simulating the effects of Indonesian fire aerosols (AERO ensemble mean minus NAERO ensemble mean). Only statistically significant (as indicated by the Student's t test) grid column differences are shown. Grey contours show AERO ensemble-mean specific humidity.

the midtroposphere to upper troposphere with the largest increase of 80 ppbv (~50%) in October just below the tropopause. It should be noted that because both the AERO and NAERO ensembles use identical CO emissions, differences in CO distributions are due only to the radiative impacts of Indonesian biomass burning aerosol.

[35] During October, decreases in CO are seen below 500 mb which is in contrast to the specific humidity profiles (Figure 10) that showed an increase in moisture at low levels. When the radiative effects of Indonesian aerosols are simulated, upward transport of CO and water vapor increases, resulting in larger mixing ratios at upper levels. At low levels, increased horizontal convergence brings moist air into the Indonesian region. However, air parcels transported into the region horizontally have lower CO mixing ratios because they have not been exposed to strong BB. As a result, CO mixing ratios in the lower troposphere decrease while water vapor increases. Water vapor profiles fail to show an upper tropospheric peak similar to those in CO profiles because the atmosphere in the UT is often near saturation, resulting in increases in upper tropospheric cloudiness as shown in Figure 6.

[36] Figure 13 shows the horizontal distribution of the change in CO resulting from aerosol heating during SON 2006. Below the tropopause, at 150 hPa, peak changes in CO exceed 70 ppbv over areas of Kalimantan and the Java Sea. Increases of up to 20 ppbv extend over the Pacific Ocean. At 100 hPa, just above the tropopause, peak CO changes are considerably smaller (~20 ppbv) and occur over the Karimata Strait. Increases greater than 10 ppbv extend over long distances in the Indian and Pacific Oceans. Changes in total CO mass in the TTL (region below the tropopause but above 150 mb), LS (region above the tropopause but below 60 hPa), and lowermost stratosphere (region above the tropopause but with potential temperature less than 380 K) in the AERO simulations were calculated following *Duncan et al.* [2007a]. Mass perturbations are calculated globally and include all latitudes and longitudes. It should be noted that the mass perturbations calculated here represent only the change resulting from simulating Indonesian aerosols and their radiative impacts; CO emissions are the same in both the AERO and NAERO ensembles and include CO produced by the Indonesian fires. Mass

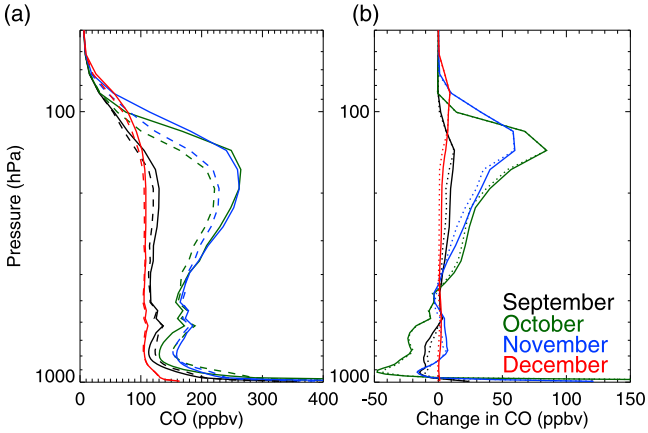

Figure 12. (a) Profiles of CO from the AERO (solid lines) and NAERO (dashed lines) ensembles and (b) changes in CO mixing ratio because of Indonesian aerosols (AERO ensemble mean minus NAERO ensemble mean) in September (black), October (green), November (blue), and December (red). Solid lines in Figure 12b indicate profiles calculated over all grid cells between 100° to 120°E and 10°S to 10°N while dotted lines indicate profiles including only grid cells in which the Student's t test indicated statistically significant differences.

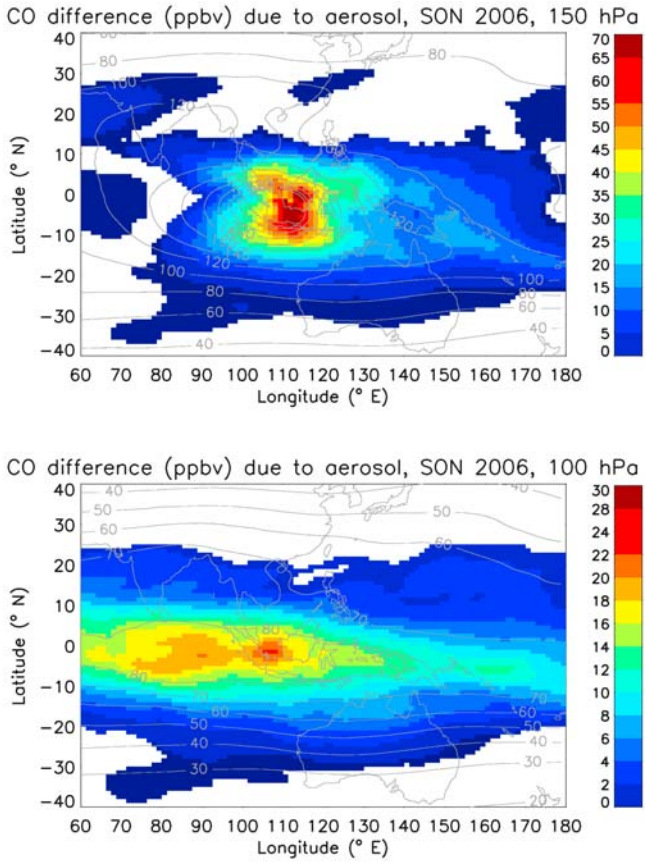

Figure 13. Average CO mixing ratio difference during SON 2006 at (top) 150 hPa and (bottom) 100 hPa resulting from simulating the effects of Indonesian biomass burning (BB) aerosols (AERO ensemble mean minus NAERO ensemble mean). Only statistically significant (as indicated by the Student's t test) grid column differences are shown. Grey contours show AERO ensemble mean CO mixing ratios.

perturbations calculated by *Duncan et al.* [2007a] included emissions from the 1997 Indonesian fires but did not include the dynamic impacts of aerosols because they were computed in an offline CTM. Increased diabatic heating and lifting associated with Indonesian aerosols increases the mass of CO in the TTL by 7% in October and 9% in November (Figure 14). Changes in the stratosphere are smaller but persist longer with changes in the LS peaking at 5% in December, at the end of the 9 month simulations.

4.6. Evolution of Changes in UTLS Dynamics

[37] Simulating the radiative effects of Indonesian BB aerosols leads to significant decreases in temperature and specific humidity at the tropopause. Figure 15 shows the daily evolution of changes in temperature, specific humidity, grid-scale vertical mass flux, horizontal divergence, cloud cover, and carbonaceous aerosol caused by the Indonesian fires. The largest increase in aerosols occurs during the period between 20 September and 10 November with a peak in aerosol mass in the UT on 28 October. The maximum aerosol mass at 850 hPa occurs in early October with a secondary maximum at the end of the month. Upward mass transport in the UT increases during this period with the largest increase occurring in early October. A small but statistically significant increase of upward mass flux also occurs at the tropopause (118 hPa). Though less statistically significant, increases in upward mass flux in the UT are accompanied by increased divergence. Daily increases in temperature in the UT are fairly constant throughout this period, ranging from 0 to 1 K per day at 300 and 200 hPa and typically less than 0.5 K per day at 150 hPa. Large episodic increases in water vapor in the UT closely follow periods of increased upward motion.

[38] Temperature changes at the tropopause and above show a higher degree of variability than those in the UT. Sharp decreases in temperature at the tropopause and increases at 85 hPa occur from 1 October to 15 October, the time period when the largest increase in upward motion occurs in the UT. During this period, convergence increases at 85 hPa and is associated with a small degree of downward motion which brings warmer stratospheric air downward, increasing temperatures at this level. Temperature decreases at the tropopause are less intuitive. Changes in the radiative heating rates (Figure 6a) indicate a small amount of net heating in the vicinity of the tropopause. An analysis of model tendency terms due to moist processes indicates that these processes have a relatively small impact on temperature in the vicinity of the tropopause meaning that the cause of these temperature decreases is likely dynamical in nature. Upward motion caused by increased buoyancy affects temperature in two ways; in the troposphere, warmer air is lofted from below which tends to increase air temperature at upper levels. At the same time, as air parcels are lifted to lower pressures, they experience adiabatic cooling. Vertical temperature advection and adiabatic cooling largely offset throughout the troposphere with the net effect on temperature governed by the difference between the environmental

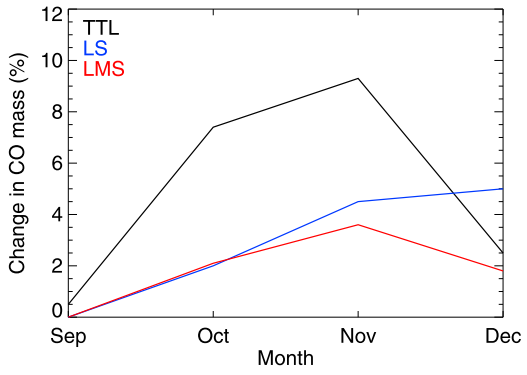

Figure 14. Monthly mass perturbation (AERO ensemble mean minus NAERO ensemble mean) in the tropical tropopause layer (TTL) (region below the tropopause but above 150 mb) (black line), lower stratosphere (LS) (region above the tropopause but below 60 hPa) (blue line), and lowermost stratosphere (region above the tropopause but with potential temperature less than 380 K) (red line) caused by Indonesian BB aerosols.

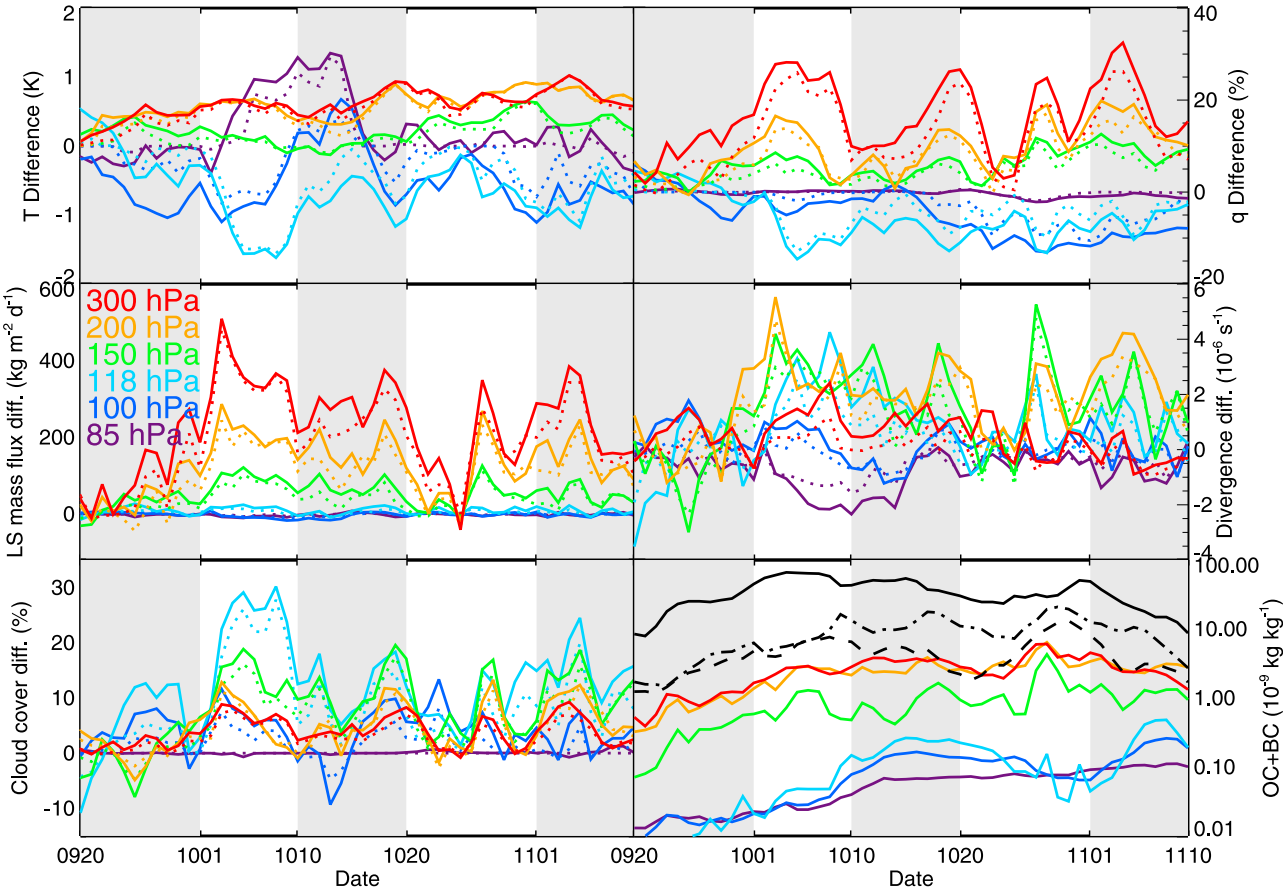

Figure 15. Daily evolution of changes in area mean temperature, specific humidity, grid-scale mass flux, horizontal divergence, cloud cover, and carbonaceous aerosol mass mixing ratio caused by Indonesian fires (AERO ensemble mean minus NAERO ensemble mean) at 300 (red lines), 200 (orange lines), 150 (green lines), 118 (light blue lines), 100 (dark blue lines), and 85 (purple lines) hPa. Carbonaceous aerosol plot also includes changes in aerosol mass mixing ratio at 850 (solid black line), 700 (dash-dot black line), and 500 (dashed black line) hPa. Solid lines indicate quantities calculated over all grid cells from 100° to 120°E and 10°S to 10°N while dotted lines indicate quantities calculated including only grid cells in which the Student's t test indicated statistically significant differences.

and dry adiabatic lapse rates. The environmental lapse rate is typically less than the dry adiabatic rate which implies net cooling in rising air parcels when diabatic changes are not considered. Throughout the troposphere, diabatic changes such as increases in short-wave heating because of aerosols dominate. At the tropopause, in the absence of strong diabatic heating changes caused by Indonesian aerosols, dynamical changes induced by the aerosols exert a stronger influence. As air is lifted near the tropopause, the environmental lapse rate becomes considerably smaller than the dry adiabatic lapse rate. In this region, rising air causes strong cooling as adiabatic cooling dominates vertical temperature advection.

[39] Decreases in water vapor occur at the tropopause in October in the same areas associated with rising air and temperature decreases. Because temperature decreases lower the saturation vapor pressure, relative humidity actually increases though the total amount of water vapor is less. This level is also where the greatest increase in cloudiness is found. The decrease in water vapor at the tropopause is approximately equal to the increase in cloud ice mass indicating that the decrease in water vapor is associated with decreases in temperature and increases in cloudiness.

5. Summary and Conclusions

[40] *Duncan et al.* [2007a] previously demonstrated that Indonesian fires in 1997 could alter the chemistry and composition of the TTL and LS using an offline CTM. Here, we present results examining the influence of aerosols produced by 2006 fires on atmospheric dynamics using ensemble simulations of the GEOS-5 AGCM which include aerosol direct and semidirect effects. Clear-sky TOA radiative forcings were as large as -30 W m^{-2} over Indonesia in October, though increases in cloud radiative forcings associated with the aerosols tend to be of opposite sign. Stronger impacts were found at the surface where clear-sky radiative forcings as low as -220 W m^{-2} were found over Indonesia.

[41] *Duncan et al.* [2003] estimated clear-sky aerosol radiative forcings at the surface as low as -178 W m^{-2}

during October 1997 over Indonesia. In the simulations of *Duncan et al.* [2003] of the 1997 event, the aerosol plume affected large areas of the Indian and Pacific Oceans with radiative forcing less than -5 W m^{-2} found as far away as Africa. In our simulations, negative peaks in radiative forcing are stronger over the burning region but the horizontal extent of the aerosol plume is considerably smaller than in the simulations of *Duncan et al.* [2003] of the 1997 event. This pattern is consistent with the GFEDv2 emissions of BC and OC. Emissions of carbonaceous aerosols from all Indonesian land regions were higher by a factor of 1.9 (4.4) in August (September) of 1997 compared to the same months in 2006. In contrast, during October, emissions were only 26% greater in 1997 than in 2006. Aerosol emissions from Kalimantan were 3.5 times greater in September 1997 than in September 2006, but during October, emissions were nearly equal in both years. Over the southwest portion of Kalimantan (south of the equator and west of 115°E) where the peak in direct aerosol radiative forcing is found in our simulations, aerosol emissions from the GFEDv2 inventory were 8% greater during October 2006 than October 1997. Though the 1997 Indonesian fires were stronger than the 2006 fires and produced more total aerosol mass, the slightly elevated emissions over southwest Kalimantan during October 2006 produce a peak radiative forcing that is comparable to the peak forcings calculated by *Duncan et al.* [2003] for the 1997 event. Because burning was significantly weaker during August and September of 2006, the area influenced by Indonesian BB aerosols during October of that year is considerably smaller than the area influenced by the 1997 event.

[42] Temperatures over Indonesia were strongly modified by increased diabatic heating during the period of burning. The largest increases were found in October and November between 150 and 400 hPa. In some regions, increases exceeded 0.7 K during SON. In addition to significant warming in the UT, aerosol heating caused strong cooling at the tropopause in October as air parcels rising in the vicinity of the tropopause experienced strong adiabatic cooling.

[43] Diabatic heating from Indonesian fire aerosols increased temperature and buoyancy throughout the troposphere in October resulting in large increases in upward motion over the region. Increases in vertical motion were accompanied by changes in the horizontal flow. Below 400 hPa, increasing convergence occurred over Indonesia while increases in divergence were found between 100 and 400 hPa. Water vapor mixing ratios increased throughout the troposphere with the largest increases in terms of percentage occurring in October at 400 hPa as stronger updrafts carried air with larger moisture contents to higher levels. In the UT, increases in water vapor are smaller than below because more water vapor is converted to cloud ice as cloud cover increases. At the tropopause and in the layer above, temperatures lowered by adiabatic cooling contribute to decreased water vapor and increased cloud formation in October.

[44] Increases in upward motion also affect the transport of BB pollution to the UTLS. CO mixing ratios are increased by over 80 ppbv (~50%) in October just below the tropopause. An analysis of CO mass indicated that aerosol heating increased the mass of CO in the TTL by 9% in November. Changes in the LS were smaller and lagged those in the TTL but in December were as large as 5%.

6. Concluding Remarks

[45] *Duncan et al.* [2007a] used an offline CTM to examine the impact of the 1997 Indonesian fires on cross-tropopause transport. Their results indicated that increased CO mixing ratios could reduce OH mixing ratios, increasing atmospheric lifetimes and troposphere-to-stratosphere transport of a number of trace gases. While the present study does not consider chemical effects, our results demonstrate that diabatic heating from Indonesian fire aerosols can strongly influence circulation and composition in the UTLS and may also play a significant role in troposphere-to-stratosphere transport. Though we have only simulated the transport of CO, it is likely that aerosol heating also influences the transport of other species produced by fire events such as CO_2, NO_x, methane and nonmethane hydrocarbons to the UTLS. It is necessary for GCMs to include realistic representations of aerosols which fully represent the interannual variability of BB emissions in order to capture these effects.

[46] It should be noted that the study presented here has several limitations. The aerosol indirect affect was not included in these simulations. *Langmann* [2007] studied the impact of aerosols from the 1997 Indonesian fires on cloud and precipitation formation (second indirect effect) using a regional climate model. Their results indicated that smoke aerosols often suppressed precipitation, resulting in increased cloud top heights for shallow clouds and decreased cloud top heights for deep convective clouds; in some cases, the presence of smoke aerosols increased precipitation and resulted in shallower low clouds and deeper convective clouds [*Langmann*, 2007]. Our results indicate that aerosol direct and semidirect effects increased cloudiness over Indonesia in 2006 with the greatest impact found in the UTLS. Further studies are needed to examine the collective impacts of direct, indirect, and semidirect effects on cloud and precipitation processes though much uncertainty remains regarding the role of aerosol indirect effects [i.e., *Intergovernmental Panel on Climate Change*, 2007].

[47] These simulations did not consider the influence of aerosols on SSTs. *Rajeev et al.* [2008] found that the 1997 Indonesian fires reduced SSTs by 1 to 2°C in the eastern equatorial Indian Ocean and suggested that the impact could potentially strengthen the Indian Ocean Dipole. The increases in cloudiness found in our ensemble simulations could also influence SSTs but studies with coupled atmosphere-ocean GCMs are needed to fully understand how aerosol-induced changes in SST drive atmospheric circulation. For simplicity, the ensemble simulations presented here used aerosol forcing fields calculated offline. Future studies will focus on understanding how changes in dynamics alter aerosol distributions through changes in horizontal and vertical advection and wet removal.

[48] This work also demonstrates the importance of ensemble simulations in understanding the role of aerosol forcing in the climate system. Ten-member ensembles were sufficient for examining changes in dynamics in the Indonesian region as indicated by statistical analysis using the Student's t test, but larger ensembles are necessary to

identify potential climate teleconnections and impacts outside of the immediate source region. As computer models increase in complexity, internal model variability is likely to increase, requiring even larger ensembles to discern statistically significant changes.

[49] **Acknowledgments.** This research was supported by NASA's Modeling, Analysis, and Prediction Program. We thank Michele Rienecker for her support and encouragement to perform this research in the Global Modeling and Assimilation Office.

References

Arakawa, A., and W. H. Schubert (1974), Interaction of a cumulus cloud ensemble with the large-scale environment, Part I, *J. Atmos. Sci.*, *31*, 674–701, doi:10.1175/1520-0469(1974)031<0674:IOACCE>2.0.CO;2.

Bian, H., M. Chin, S. R. Kawa, B. Duncan, A. Arellano, and P. Kasibhatla (2007), Sensitivity of global CO simulations to uncertainties in biomass burning sources, *J. Geophys. Res.*, *112*, D23308, doi:10.1029/2006JD008376.

Chandra, S., J. R. Ziemke, B. N. Duncan, T. L. Diehl, N. J. Livesey, and L. Froidevaux (2009), Effects of the 2006 El Niño on tropospheric ozone and carbon monoxide: Implications for dynamics and biomass burning, *Atmos. Chem. Phys.*, *9*, 4239–4249, doi:10.5194/acp-9-4239-2009.

Chin, M., P. Ginoux, S. Kinne, B. N. Holben, B. N. Duncan, R. V. Martin, J. A. Logan, A. Higurashi, and T. Nakajima (2002), Tropospheric aerosol optical thickness from the GOCART model and comparisons with satellite and sunphotometer measurements, *J. Atmos. Sci.*, *59*, 461–483, doi:10.1175/1520-0469(2002)059<0461:TAOTFT>2.0.CO;2.

Chin, M., T. Diehl, O. Dubovik, T. F. Eck, B. N. Holben, A. Sinyuk, and D. G. Streets (2009), Light absorption by pollution, dust, and biomass burning aerosols: A global model study and evaluation with AERONET measurements, *Ann. Geophys.*, *27*, 3439–3464.

Chou, M.-D., and M. J. Suarez (1994), An efficient thermal infrared radiation parameterization for use in general circulation models, *NASA Tech. Memo*, *TM-104606*, vol. *3*, 85 pp.

Chou, M.-D., and M. J. Suarez (2002), A solar radiation parameterization for atmospheric studies, *NASA Tech. Memo*, *TM-104606*, vol. *15*, 40 pp.

Chou, M.-D., M. J. Suarez, X.-A. Liang, and M. M.-H. Yan (2003), A thermal infrared radiation parameterization for atmospheric studies, *NASA Tech. Memo*, *TM-104606*, vol. *19*, 85 pp.

Chung, C. E., and V. Ramanathan (2006), Weakening of north Indian SST gradients and the monsoon rainfall in India and the Sahel, *J. Clim.*, *19*, 2036–2045, doi:10.1175/JCLI3820.1.

Dickerson, R. R., S. Kondragunta, G. Stenchikov, K. L. Civerolo, B. G. Doddridge, and B. Holben (1997), The impact of aerosols on solar UV radiation and photochemical smog, *Science*, *278*(5339), 827–830, doi:10.1126/science.278.5339.827.

Duncan, B. N., and J. A. Logan (2008), Model analysis of the factors regulating the trends and variability of carbon monoxide between 1988 and 1997, *Atmos. Chem. Phys.*, *8*, 7389–7403, doi:10.5194/acp-8-7389-2008.

Duncan, B. N., R. V. Martin, A. C. Staudt, R. Yevich, and J. A. Logan (2003), Interannual and seasonal variability of biomass burning emissions constrained by satellite observations, *J. Geophys. Res.*, *108*(D2), 4100, doi:10.1029/2002JD002378.

Duncan, B. N., S. E. Strahan, Y. Yoshida, S. D. Steenrod, and N. Livesey (2007a), Model study of the cross-tropopause transport of biomass burning pollution, *Atmos. Chem. Phys.*, *7*, 3713–3736, doi:10.5194/acp-7-3713-2007.

Duncan, B. N., J. A. Logan, I. Bey, I. A. Megretskaia, R. M. Yantosca, P. C. Novelli, N. B. Jones, and C. P. Rinsland (2007b), The global budget of CO, 1988–1997: Source estimates and validation with a global model, *J. Geophys. Res.*, *112*, D22301, doi:10.1029/2007JD008459.

Field, R. D., G. R. van der Werf, and S. S. P. Shen (2009), Human amplification of drought-induced biomass burning in Indonesia since 1960, *Nat. Geosci.*, *2*, doi:10.1038/ngeo443.

Guenther, A., et al. (1995), A global model of natural volatile organic compound emissions, *J. Geophys. Res.*, *100*, 8873–8892, doi:10.1029/94JD02950.

Hargreaves, J. C., A. Abe-Ouchi, and J. D. Annan (2007), Linking glacial and future climates through an ensemble of GCM simulations, *Clim. Past*, *3*, 77–87, doi:10.5194/cp-3-77-2007.

Huebener, H., U. Cubasch, U. Langematz, T. Spangehl, F. Niehörster, I. Fast, and M. Kunze (2007), Ensemble climate simulations using a fully coupled ocean-troposphere-stratosphere general circulation model, *Philos. Trans. R. Soc. A*, *15*, 365, doi:10.1098/rsta.2007.2078.

Intergovernmental Panel on Climate Change (2007), *Climate Change 2007: Synthesis Report. Contribution of Working Group I to the Fourth Assessment Report of the Intergovernmental Panel on Climate Change*, edited by S. Solomon et al., Cambridge Univ. Press., New York.

Jaenicke, J., et al. (2008), Determination of the amount of carbon stored in Indonesian peatlands, *Geoderma*, *147*, 151–158, doi:10.1016/j.geoderma.2008.08.008.

Jiang, J. H., et al. (2010), Five-year (2004–2009) observations of upper tropospheric water vapor and cloud ice from MLS and comparisons with GEOS-5 analyses, *J. Geophys. Res.*, doi:10.1029/2009JD013256, in press.

Koster, R. D., M. J. Suarez, A. Ducharne, M. Stieglitz, and P. Kumar (2000), A catchment-based approach to modeling land surface processes in a general circulation model 1. Model structure, *J. Geophys. Res.*, *105*, 24,809–24,822, doi:10.1029/2000JD900327.

Langmann, B. (2007), A model study of smoke-haze influence on clouds and warm precipitation formation in Indonesia 1997/1998, *Atmos. Environ.*, *41*, doi:10.1016/j.atmosenv.2007.04.050.

Lau, K.-M., and K.-M. Kim (2006), Observational relationships between aerosol and Asian monsoon rainfall, and circulation, *Geophys. Res. Lett.*, *33*, L21810, doi:10.1029/2006GL027546.

Lau, K. M., M. K. Kim, and K. M. Kim (2006), Asian monsoon anomalies induced by aerosol direct effects, *Clim. Dyn.*, *26*, 855–864, doi:10.1007/s00382-006-0114-z.

Li, Z. X. (1999), Ensemble atmospheric GCM simulation of climate interannual variability from 1979 to 1994, *J. Clim.*, *12*, 986–1001, doi:10.1175/1520-0442(1999)012<0986:EAGSOC>2.0.CO;2.

Lin, S.-J. (2004), A "vertically Lagrangian" finite-volume dynamical core for global models, *Mon. Weather Rev.*, *132*(10), 2293–2307, doi:10.1175/1520-0493(2004)132<2293:AVLFDC>2.0.CO;2.

Livesey, N. J., et al. (2008), Validation of Aura Microwave Limb Sounder O3 and CO observations in the upper troposphere and lower stratosphere, *J. Geophys. Res.*, *113*, D15S02, doi:10.1029/2007JD008805.

Lock, A. P., A. R. Brown, M. R. Bush, G. M. Martin, and R. N. B. Smith (2000), A new boundary layer mixing scheme. Part I: Scheme description and single-column model tests, *Mon. Weather Rev.*, *128*, 3187–3199, doi:10.1175/1520-0493(2000)128<3187:ANBLMS>2.0.CO;2.

Logan, J. A., I. Megretskaia, R. Nassar, L. T. Murray, L. Zhang, K. W. Bowman, H. M. Worden, and M. Luo (2008), Effects of the 2006 El Niño on tropospheric composition as revealed by data from the Tropospheric Emission Spectrometer (TES), *Geophys. Res. Lett.*, *35*, L03816, doi:10.1029/2007GL031698.

Menon, S., J. E. Hansen, L. Nazarenko, and Y. Luo (2002), Climate effects of black carbon aerosols in China and India, *Science*, *297*, 2250–2253, doi:10.1126/science.1075159.

Ming, Y., and V. Ramaswamy (2009), Nonlinear climate and hydrological responses to aerosol effects, *J. Clim.*, *22*, 1329–1339, doi:10.1175/2008JCLI2362.1.

Moorthi, S., and M. J. Suarez (1992), Relaxed Arakawa-Schubert: A parameterization of moist convection for general circulation models, *Mon. Weather Rev.*, *120*, 978–1002, doi:10.1175/1520-0493(1992)120<0978:RASAPO>2.0.CO;2.

Page, S. E., F. Siegert, J. O. Rieley, H.-D. V. Boehm, A. Jaya, and S. Limin (2002), The amount of carbon released from peat and forest fires in Indonesia during 1997, *Nature*, *420*, doi:10.1038/nature01131.

Podgorny, I. A., F. Li, and V. Ramanathan (2003), Large aerosol radiative forcing due to the 1997 Indonesian forest fire, *Geophys. Res. Lett.*, *30*(1), 1028, doi:10.1029/2002GL015979.

Rajeev, K., K. Parameswaran, S. K. Nair, and S. Meenu (2008), Observational evidence for the radiative impact of Indonesian smoke in modulating the sea surface temperature of the equatorial Indian Ocean, *J. Geophys. Res.*, *113*, D17201, doi:10.1029/2007JD009611.

Ramanathan, V., and P. J. Crutzen (2003), New directions: Atmospheric brown "clouds", *Atmos. Environ.*, *37*(28), 4033–4035, doi:10.1016/S1352-2310(03)00536-3.

Ramaswamy, V., et al. (2001), Radiative forcing of climate change, in *Climate Change 2001*, edited by J. T. Houghton et al., pp. 239–287, Cambridge Univ. Press, New York.

Randles, C. A., and V. Ramaswamy (2008), Absorbing aerosols over Asia: A Geophysical Fluid Dynamics Laboratory general circulation model sensitivity study of model response to aerosol optical depth and aerosol absorption, *J. Geophys. Res.*, *113*, D21203, doi:10.1029/2008JD010140.

Reinecker, M. M., et al. (2008), The GEOS-5 Data Assimilation System-Documentation of versions 5.0.1, 5.1.0, and 5.2.0, *NASA Tech. Rep. 104606 V27*.

Reynolds, R. W., T. M. Smith, C. Liu, D. B. Chelton, K. S. Casey, and M. G. Schlax (2007), Daily high-resolution blended analyses for sea surface temperature, *J. Clim.*, *20*, 5473–5496, doi:10.1175/2007JCLI1824.1.

Rudich, Y., A. Sagi, and D. Rosenfeld (2003), The influence of the Kuwait oil fires plume (1991) on the microphysical development of clouds, *J. Geophys. Res.*, *108*(D15), 4478, doi:10.1029/2003JD003472.

Schwartz, M. J., et al. (2008), Validation of the Aura Microwave Limb Sounder temperature and geopotential height measurements, *J. Geophys. Res.*, *113*, D15S11, doi:10.1029/2007JD008783.

Taschetto, A. S., and M. H. England (2008), Estimating ensemble size requirements of AGCM simulations, *Meteorol. Atmos. Phys.*, *100*, 23–36, doi:10.1007/s00703-008-0293-8.

Thampi, B. V., K. Rajeev, K. Parameswaran, and M. K. Mishra (2009), Spatial distribution of the southeast Asian smoke plume over the Indian Ocean and its radiative heating in the atmosphere during the major fire event of 2006, *Geophys. Res. Lett.*, *36*, L16808, doi:10.1029/2009GL039316.

van der Werf, G. R., J. T. Randerson, G. J. Collatz, and L. Giglio (2003), Carbon emissions from fires in tropical and subtropical ecosystems, *Global Change Biol.*, *9*(4), 547–562, doi:10.1046/j.1365-2486.2003.00604.x.

van der Werf, G. R., J. T. Randerson, L. Giglio, G. J. Collatz, P. S. Kasibhatla, and A. F. Arellano Jr. (2006), Interannual variability in global biomass burning emissions from 1997 to 2004, *Atmos. Chem. Phys.*, *6*, 3423–3441, doi:10.5194/acp-6-3423-2006.

Vitart, F., J. L. Anderson, and W. F. Stern (1997), Simulation of interannual variability of tropical storm frequency in an ensemble of GCM integrations, *J. Clim.*, *10*, 745–760, doi:10.1175/1520-0442(1997)010<0745:SOIVOT>2.0.CO;2.

Wang, Y., R. D. Field, and O. Roswintiarti (2004), Trends in atmospheric haze induced by peat fires in Sumatra Island, Indonesia and El Niño phenomenon from 1973 to 2003, *Geophys. Res. Lett.*, *31*, L04103, doi:10.1029/2003GL018853.

Wehner, M. F. (2000), A method to aid in the determination of the sampling of AGCM ensemble simulations, *Clim. Dyn.*, *16*, 321–331, doi:10.1007/s003820050331.

Yevich, R., and J. A. Logan (2003), An assessment of biofuel use and burning of agricultural waste in the developing world, *Global Biogeochem. Cycles*, *17*(4), 1095, doi:10.1029/2002GB001952.

Yu, H., M. Chin, D. M. Winker, A. H. Omar, Z. Liu, C. Kittaka, and T. Diehl (2010), Global view of aerosol vertical distributions from CALIPSO lidar measurements and GOCART simulations: Regional and seasonal variations, *J. Geophys. Res.*, doi:10.1029/2009JD013364, in press.

Zhu, Y., and R. Gelaro (2008), Observation sensitivity calculations using the adjoint of the Gridpoint Statistical Interpolation (GSI) analysis system, *Mon. Weather Rev.*, *136*, 335–351, doi:10.1175/MWR3525.1.

Ziemke, J. R., S. Chandra, B. N. Duncan, M. R. Schoeberl, O. Torres, M. R. Damon, and P. K. Bhartia (2009), Recent biomass burning in the tropics and related changes in tropospheric ozone, *Geophys. Res. Lett.*, *36*, L15819, doi:10.1029/2009GL039303.

M. Chin, P. Colarco, and B. Duncan, Atmospheric Chemistry and Dynamics Branch, NASA Goddard Space Flight Center, Greenbelt, MD 20771, USA.

T. Diehl, L. Ott, and C. Randles, Goddard Earth Sciences and Technology Center, University of Maryland, Greenbelt, MD 2077, USA. (lesley.e.ott@nasa.gov)

E. Nielsen, Science Systems and Applications, Inc., 10210 Greenbelt Rd., Suite 600, Lanham, MD 20706, USA.

S. Pawson, Global Modeling and Assimilation Office, NASA Goddard Space Flight Center, Greenbelt, MD 20706, USA.